Journal of Radioanalytical and Nuclear Chemistry (2021) 330:225–235
https://doi.org/10.1007/s10967-021-07952-0

Investigation of the adsorption properties of U(VI) by sulfonic acid-functionalized carbon materials

Bao Yunyun[1] · Chao Jiang[1] · Yan Liu[1] · Changfu Wang[1] · Jinbiao Liu[2]

Received: 30 May 2021 / Accepted: 13 August 2021 / Published online: 29 August 2021

Abstract
In this study, sulfonic acid-functionalized carbon materials (CS-SO_3H) was carbonized and functionalized by polyphosphazene (PZS). The morphology and structure were characterized by FTIR, XPS and SEM. The influences of pH, contact time, initial concentration and temperature of CS-SO_3H for uranyl ions were investigated. Results indicated that the adsorption equilibrium time was about 20 min. The adsorption process was more consistent with the Langmuir isotherm and the pseudo-second-order model. In addition, the maximum adsorption capacity of CS-SO_3H was about 341.98 mg/g. Moreover, the thermodynamic parameters of ΔG, ΔH and ΔS show that the uranium adsorption process was spontaneous and endothermic.

Keywords Polyphosphazene · Sulfonic acid-functionalized · Carbon materials · Uranium · Adsorption

Introduction

In order to alleviate the pressure caused by the energy crisis [1, 2], more and more countries begin to look for new clean energy to replace the original fossil energy. To this end, nuclear power is promising, with uranium is one of the key raw materials [3–5]. However, due to uranium's inherent high hydrophilicity and long half-life, it has increasingly been considered to be a serious menace to the human health and ecological environment [6–10]. Consequently, it is of vital importance to develop reliable and effective methods to treat uranium-containing wastewater from uranium mines and nuclear facilities [5, 11, 12].

Uranium has five oxidation states, and mainly exists in the form of U(IV) and U(VI) in water [13]. U(IV) is generally removed from water in the form of precipitation. In contrast, U(VI) has good solubility in aqueous solution and is not easy to precipitate. As a result, in order to remove U(VI) from aqueous solution, different methods have been developed and adopted, including chemical precipitation [14], membrane separation [15], ion exchange [16], reverse osmosis [17], adsorption and so on. Among these methods, adsorption has advantages of wide application range, effective treatment, economical, and availability of different adsorbents. Some adsorbents, such as polypyrrole [13], chitosan [18] and polyethylene fiber [19], have been successfully utilized to remove U(VI) from aqueous solution.

Carbon materials, including activated carbon [20–22], carbon aerogel [23, 24], graphene oxide [25] and carbon nanotube [26], exhibit good adsorption performance. These are ideal heavy metal adsorption materials, because of high porosity, low density, high specific surface area, chemical stability, high temperature resistance and some mechanical strength [27]. However, traditional carbon materials lack functional groups on the surface and generally exhibit poor adsorption capacity [28]. In particular, soft donor atoms such as nitrogen and sulfur are crucial in actinide-lanthanide separation because these elements preferentially bond to ligands containing the soft donor atoms [29].

Polyphosphazene, a new type of functional hybrid material with unique P = N structure unit and active P-Cl groups, refers to polymers synthesized by condensation reaction between hexachlorocytriphosphazene (HCCP) and other monomers [30, 31]. The polymer has a stable six-membered ring conjugate structure, but does not form conjugate in long range, and thus it has a pliable P-N chain, which acts as a

✉ Yan Liu
fzliuyan1986@163.com

✉ Changfu Wang
wangcf@ecut.edu.cn

[1] State Key Laboratory of Nuclear Resources and Environment, East China University of Technology, Nanchang 330013, Jiangxi, China

[2] Department of Chemistry, Jiangxi University of Science and Technology, Ganzhou 341000, Jiangxi, China

good precursor for the preparation of carbon materials [32]. In addition, compared with traditional adsorption materials, it has the advantages of larger specific surface area, smaller size and modifiability of surface functional groups.

In this study, our specific aims were to (1) utilize polyphosphazene as the precursor to carbonize and synthesize carbon sphere (CS); (2) prepare heteroatoms doped sulfonated carbon material (CS-SO_3H) by sulfuric acid modification; (3) characterize the materials by means of FTIR, XPS and SEM; (4) explore the adsorption performance of CS-SO_3H in different pH, adsorption time, initial concentration of uranium and temperature; and (5) discuss the adsorption mechanism.

Experiments

Materials

The materials, namely, hexachlorocytriphosphazene (HCCP, $C_{16}N_3P_3$), chloroacetic acid ($C_2H_3ClO_2$), anhydrous sodium acetate ($C_2H_3NaO_2$), uranyl nitrate ($UO_2(NO_3)_2{\cdot}6H_2O$) and arsenazo III ($C_{22}H_{18}As_2N_4O_{14}S_2$) were obtained from Aladdin Chemistry Co., Ltd., China. The others, including 4,4-Sulfonyldiphenol (BPS, $C_{12}H_{10}O_4S$), triethylamine (TEA, $(C_2H_5)_3$ N), sodium hydroxide (NaOH), acetonitrile (C_2H_3N), anhydrous ethanol (C_2H_6O) and concentrated sulfuric acid (H_2SO_4) were obtained from Xilong Scientific Co., Ltd., China. All the materials above were Analytical reagent (AR) grade.

Synthesis of CS

The steps are demonstrated in Scheme 1. Firstly, under ultrasonic agitation (190 W, 40 Hz), adding 0.1217 g HCCP and 0.2628 g BPS into 100 mL acetonitrile for dispersion. After 10 min, 3 mL triethylamine was added drop-wise to the solution. The reaction continued for 3 h at 40 ℃. The white powdery substance (PZS) was obtained through centrifugation, rinsed with anhydrous ethanol and deionized water, and dried.

In an atmospheric tube furnace, the white powdery PZS powder was calcined by heating to 750 ℃ at a rate of 5 ℃/min for 2 h under a nitrogen blanket. After grinding and crushing, the black carbonaceous solid powder (CS) was acquired.

Synthesis of CS-SO_3H

100 mg as-prepared CS powder and 5 mL concentrated sulfuric acid were added into a beaker, magnetically stirred for 30 min until the CS material was evenly distributed, and then the solution was added into a 100 mL Teflon-lined stainless steel autoclave for 12 h at 120 ℃. After cooling to room temperature, the product was rinsed with anhydrous ethanol and deionized water to neutrality. The black solid powder (CS-SO_3H) was obtained after drying at 60 ℃ for 8 h in a vacuum oven.

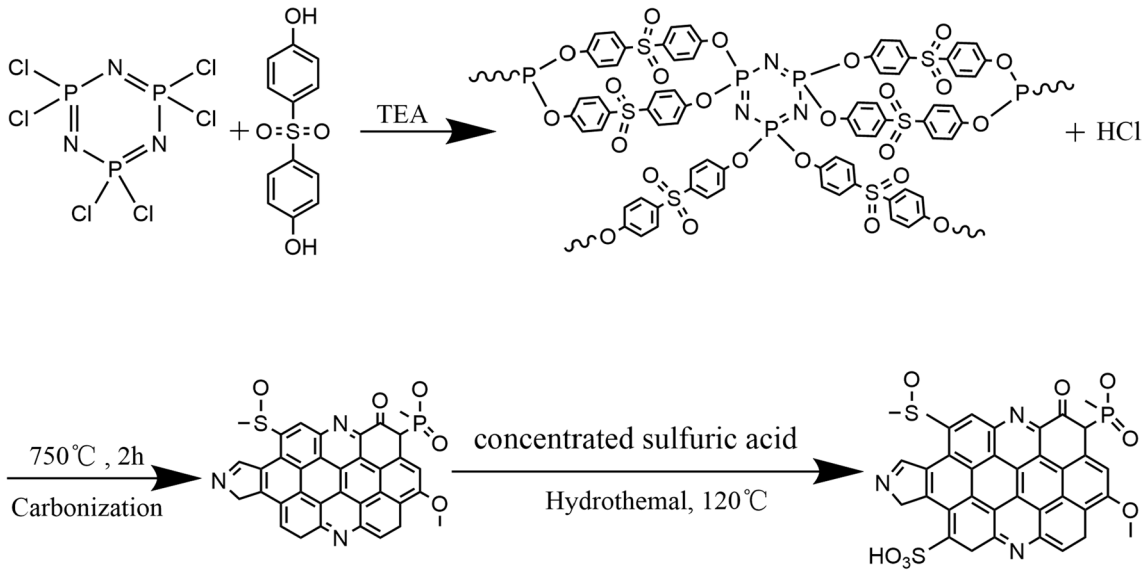

Scheme 1 Synthesis route of CS-SO_3H

Characterization

To analyze the chemical structure, the Fourier Transform Infrared Spectroscopy (FTIR) in the range of 4000–400 cm^{-1} were recorded on a TENSOR27 FTIR spectra (Bruker). The surface morphological analysis of the CS and CS-SO_3H were carried out by JEOL JSM-5900 Scanning Electron Microscopy (SEM). Also, to investigate the chemical binding energies, X-ray Photoelectron Spectra (XPS) analysis of the products were conducted using a kratos Axis Ultra DLD, and the reference was C1s lined at 284.8 eV. Brunauer–Emmett–Teller (BET) surface areas were investigated from nitrogen adsorption–desorption isotherms on a V-Sorb 2800TP specific surface area and aperture analyzer.

Adsorption experimental procedure

The performance of CS and CS-SO_3H were characterized by UV–VIS (757CRT, Tianjin Guanze Technol. Co., Ltd). In an Erlenmeyer flask, 5 mg adsorbent was added and evenly distributed into 30 mL U(VI) solution, and adjusted with 0.1 mol/L hydrochloric acid and 0.1 mol/L sodium hydroxide to achieve the targeted pH. The mixture was agitated and then filtered. The U(VI) concentration of the supernatant was obtained by the arsenazo (III) method at 650 nm with a spectrophotometer. The adsorption capacity (q_e, mg/g) for U(VI) ions was calculated according to the following equation:

$$q_e = \frac{(C_0 - C_e)V}{m} \quad (1)$$

where C_0 and C_e (mol/L) are the initial and equilibrium concentrations of the solution, respectively; V (mL) is the volume of the uranium solution; and m (mg) is the mass of the adsorbent.

Results and discussion

Characterization

FTIR

The FTIR spectra of CS and CS-SO_3H were investigated in the range of 4000–400 cm^{-1}, as exhibited in Fig. 1a. The results illustrate that the characteristic peak of CS at 1595 cm^{-1} corresponds to the stretching vibration of C=C, and the peaks at 1100 cm^{-1} and 1009 cm^{-1} correspond to the Ar–O–P bond, which indicates that condensation polymerization between raw materials has occurred. The bands of CS at 1400, 1257 and 1105 cm^{-1} are assigned to the stretching vibrations of C–N, S–O and P=O, respectively [33]. Concerning the FTIR spectrum of CS-SO_3H, new peaks at 1156 and 1033 cm^{-1} emerged, which represent the symmetric and anti-symmetric stretching vibration of S=O, while the peak at 726 cm^{-1} corresponds to the bending vibration of O–H in the sulfonic acid group, indicating that CS had been successfully sulfonated [34, 35].

The FTIR spectrum of CS-SO_3H after adsorption (namely, CS-SO_3H-U) was also studied, as presented in Fig. 1b. Compared with CS-SO_3H, the characteristic peak at 879 cm^{-1} can be attributed to the stretching vibration of the linear structure of $[O=U=O]^{2+}$. In addition, the peaks of S=O in the curve of CS-SO_3H-U are less intense than those of CS-SO_3H, reflecting the chemical bonds between uranyl ions and ligands on CS-SO_3H are successfully formed.

XPS

As in Fig. 2, XPS was used to analyze the chemical structures of CS and CS-SO_3H. According to the spectral figures, the peaks of CS at 134.3, 163.9, 284.8, 400.8, and 532.9 eV belong to P2p, S2p, C1s, N1s, and O1s, respectively. After functionalization, the intensity of O1s and

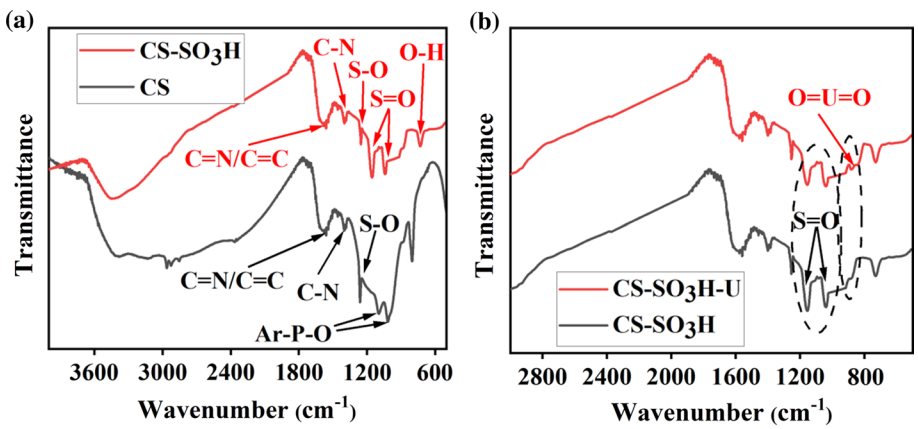

Fig. 1 (**a**) FTIR spectra of CS and CS-SO_3H; (**b**) FTIR spectra of CS-SO_3H and CS-SO_3H-U

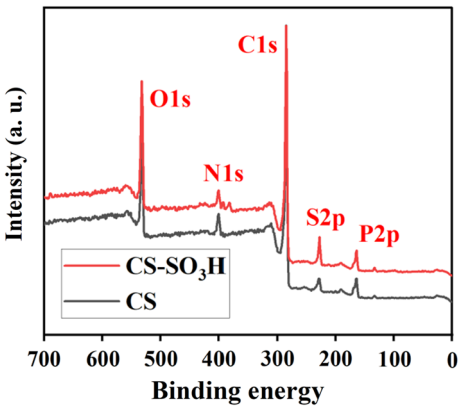

Fig. 2 The XPS images of CS and CS- SO_3H

S2p peaks increased significantly owing to the introduction of -SO_3H functional groups. This demonstrates that the functionalized material was prepared successfully.

Table 1 Pore structure data of CS and CS-SO_3H

Adsorbent	Pore volume (cm^3/g)	Specific surface area (m^2/g)	Average pore diameter (nm)
CS	0.3904	1275.54	3.618
CS-SO_3H	0.1656	1113.66	8.541

SEM

The microstructures of CS and CS-SO_3H were investigated using SEM. As observed in Fig. 3a, CS had a rough surface, porous structure and relatively uniform pore size distribution. Comparatively, the pores on the surface of CS-SO_3H increased obviously and the continuous surface disappeared (Fig. 3b), thereby increasing the contact with uranyl ions.

N_2 adsorption–desorption isotherms

The N_2 adsorption–desorption technique was used to characterize the specific surface area and pore size distribution of CS and CS-SO_3H. As shown in Fig. 4, the adsorption

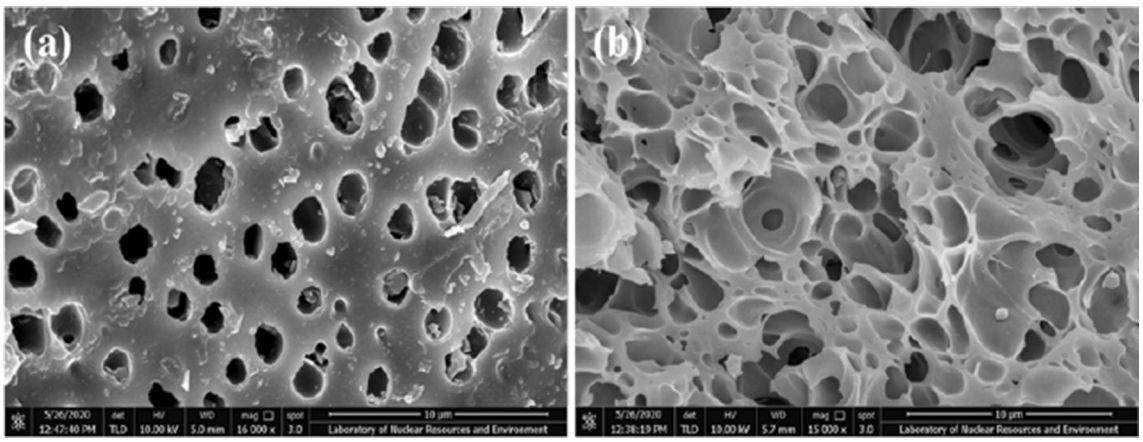

Fig. 3 The SEM images of (**a**) CS and (**b**) CS-SO_3H

Fig. 4 N_2 adsorption–desorption isotherms of CS-SO_3H

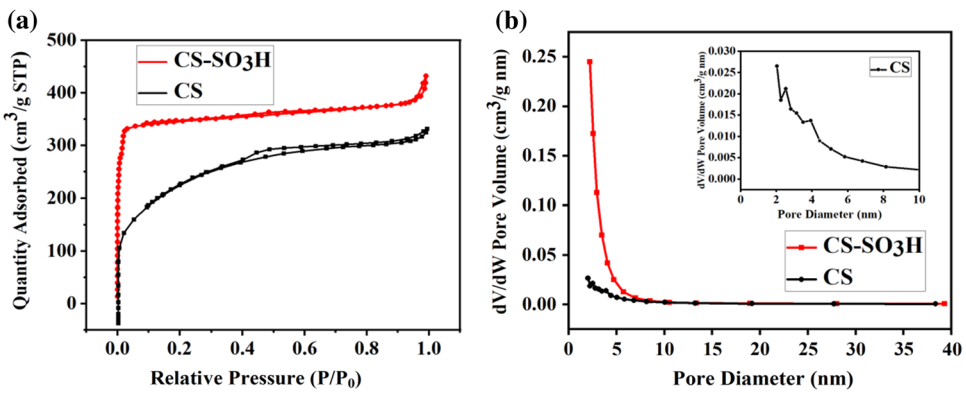

quantity in the low relative pressure area indicated the existence of micropores. The detailed pure structure data was presented in Table1. The surface area, pore-volume, and average diameter of CS-SO_3H are 1113.66 m^2/g, 0.1656 cm^3/g and 8.540 nm, respectively. The large surface area and the presence of a large number of pores can provide abundant active sites for the adsorption of uranyl ions. In addition, though surface area of CS-SO_3H was lower than CS, the the adsorption quantity of CS-SO_3H was larger, which may caused by the functionalization process by sulfonic acid.

Effect of pH

Adsorption performance is typically affected by pH. Hence, it is necessary to discuss the influence of the initial pH value on the properties of the two adsorbents. Figure 5 shows that, the adsorption capacity of uranium (VI) by CS and CS-SO_3H increased with pH increasing from 2 to 6. At the optimal pH of 6, the maximum adsorption capacity increased from 150.13 mg/g to 186.12 mg/g after introducing functional groups. For pH higher than 6, the adsorption capacity decreased with pH.

The increasing capacity with pH at low pH values can be attributed to the replacement of H_3O^+ in the binding sites with uranyl ions. When the pH value was higher than 6, the uranyl hydrates (such as $UO_2(OH)_4^{2-}$, $UO_2(OH)_3^-$ and $(UO_2)_3(OH)_7^-$) increased, which would reduce the adsorption capacity.

Adsorption kinetics

The uranium (VI) adsorption capacities of CS and CS-SO_3H with time are presented in Fig. 6, showing the rates of increase and the equilibrium capacities of the two materials were different. CS-SO_3H quickly reached a higher equilibrium capacity within 20 min, while CS at about 80 min. This

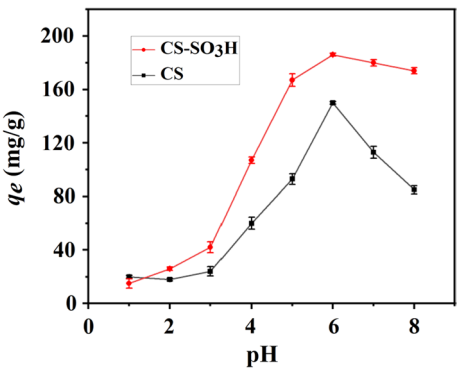

Fig. 5 Effect of initial solution pH on U(VI) adsorption by CS and CS-SO_3H

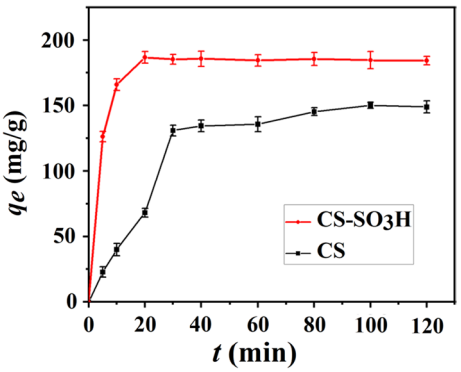

Fig. 6 Influence of contact time on U(VI) adsorption by CS and CS-SO_3H

is attributed to the higher availability of adsorption sites in CS-SO_3H.

In order to explore the uranium (VI) adsorption kinetics of CS and CS-SO_3H, pseudo-first-order and pseudo-second-order kinetic models were adopted to best-fit the experimental data:

$$\ln(q_e - q_t) = \ln\ q_e - k_1 t \tag{2}$$

$$\frac{t}{q_t} = \frac{1}{k_2 q_e^2} + \frac{1}{q_e} t \tag{3}$$

where q_t (mg/g) is the amount of uranyl ions adsorbed at time t; k_1 (min^{-1}) and k_2 (mg^{-1} min^{-1}) are the rate constants of pseudo-first-order and pseudo-second-order, respectively.

By analyzing the plots in Fig. 7, the model parameters can be obtained, as listed in Table 2. The data show that the correlation coefficients R^2 of CS and CS-SO_3H are higher for the pseudo-second-order model (0.9764 and 0.9996, respectively) than the pseudo-first-order model (0.9047 and 0.2442, respectively). This reveals that the adsorption processes were dominated by chemical adsorption in both materials.

Effect of initial concentration of uranium

The effects of initial concentration (C_0) of uranium (VI) on the adsorption by CS and CS-SO_3H at the optimum pH of 6 are illustrated in Fig. 8. At low initial concentrations, the adsorption capacities of CS and CS-SO_3H increased steeply than more gently as C_0 increased. The increase indicates that more adsorption sites are available than uranyl ions, while the slower rate of increase indicates the increasing saturation of the adsorption sites. For CS, the maximum capacity (227.68 mg/g) was at $C_0 = 80$ mg/L, and further increase in C_0 did not increase the adsorption capacity because all adsorption sites were saturated.

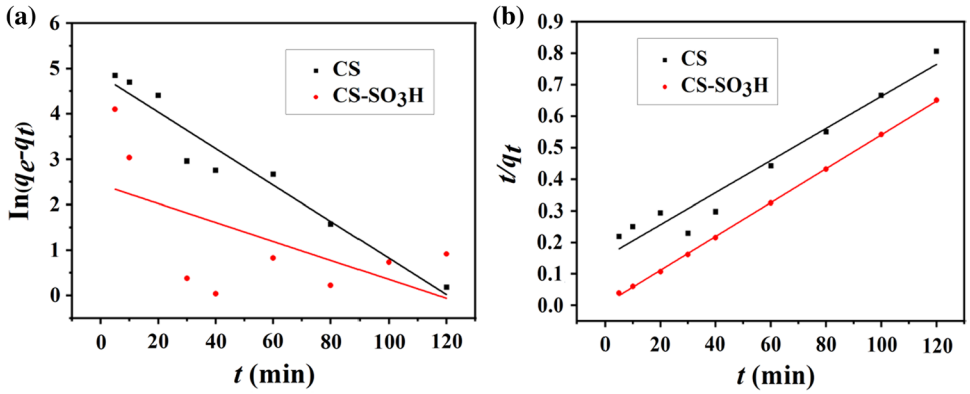

Fig. 7 (**a**) Pseudo–first–order and (**b**) pseudo–second–order adsorption kinetics of U(VI) by CS and CS-SO_3H

Table 2 Kinetic parameters of pseudo–first–order and pseudo–second–order kinetic models of U(VI) by CS and CS-SO_3H

Materials	$q_{e,exp}$ (mg/g)	Pseudo–first–order model			Pseudo–second–order model		
		$q_{1,cal}$ (mg/g)	k_1 (min^{-1})	R^2	$q_{2,cal}$ (mg/g)	k_2 ($g \cdot mg^{-1} \cdot min^{-1}$)	R^2
CS	150.13	98.69	8.21×10^{-3}	0.9047	173.31	2.88×10^{-4}	0.9764
CS-SO_3H	186.74	11.51	2.09×10^{-2}	0.2442	186.57	6.34×10^{-3}	0.9996

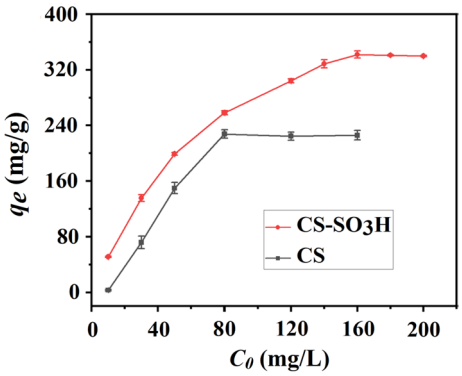

Fig. 8 Influence of initial concentration of solution on U(VI) adsorption by CS and CS-SO_3H at pH = 6

On the other hand, for CS-SO_3H, the adsorption capacity continuously increased with C_0 up to 160 mg/L and equilibrated at a higher capacity (341.98 mg/g) than CS. This reveals that the successful sulfonation of CS-SO_3H endowed the surface of materials with more functional groups, which increased the adsorption sites and caused the maximum adsorption to be higher for CS-SO_3H.

Adsorption isotherms

The equilibrium adsorption isotherm was investigated to further understand the adsorption mechanism. In this study, the Langmuir and Freundlich adsorption isotherm equations were employed to fit and analyze the experimental data:

$$\frac{C_e}{q_e} = \frac{1}{q_m K_L} + \frac{C_e}{q_m} \tag{4}$$

$$\ln\ q_e = \ln\ K_F + \frac{1}{n} \ln\ C_e \tag{5}$$

where C_e (mg/L) is the solution concentration at equilibrium; q_m (mg/g) is the maximum capacity; q_e (mg/g) is the equilibrium capacity; K_L (L/mg) and K_F are the Langmuir and Freundlich constants, respectively; and n represents the equilibrium concentration dependence of the adsorption process. For Langmuir, K_L and q_m can respectively be calculated from the intercept and slope of the plot of C_e/q_e versus C_e. In the same way, for Freundlich, $K_F$and n can be obtained from the plot of ln q_e versus ln C_e. The results are presented in Fig. 9 and Table 3.

It is evident from Table 3 that both the adsorption processes of CS and CS-SO_3H were in better agreement with the Langmuir adsorption isotherm ($R^2 = 0.9976$ and $R^2 = 0.9979$, respectively), rather than the Freundlich adsorption isotherm ($R^2 = 0.9423$ and $R^2 = 0.9651$, respectively), suggesting monolayer coverage of uranium. As calculated from the Langmuir adsorption isotherm, the maximum adsorption amounts of CS and CS-SO_3H were 229.36 mg/g and 355.87 mg/g, respectively. This shows that CS-SO_3H showed a higher

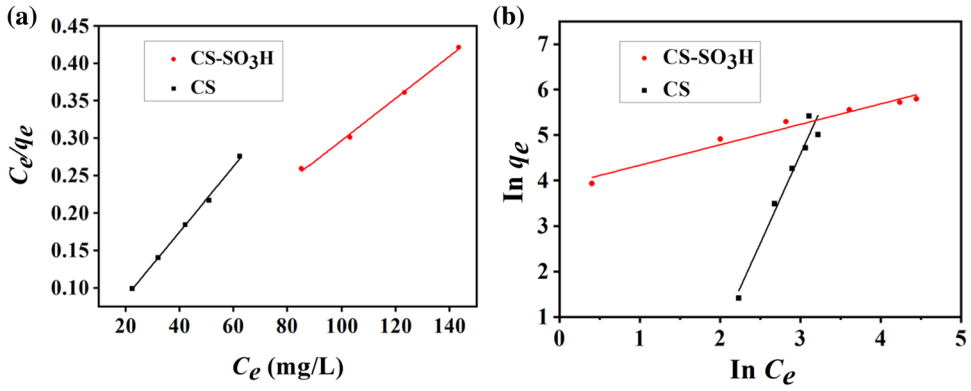

Fig. 9 (1) Langmuir and (2) Freundlich isotherms of U(VI) adsorbed by CS and CS-SO_3H

Table 3 Langmuir and Freundlich isothermal adsorption fitting parameters of CS and CS-SO_3H adsorbed uranium

Materials	Langmuir isotherm			Freundlich isotherm		
	K_L	q_m(mg/g)	R^2	K_F	n	R^2
CS	7.80	229.36	0.9976	4.05×10^{-3}	0.31	0.9423
CS-SO_3H	0.1766	355.87	0.9979	48.7078	2.22	0.9651

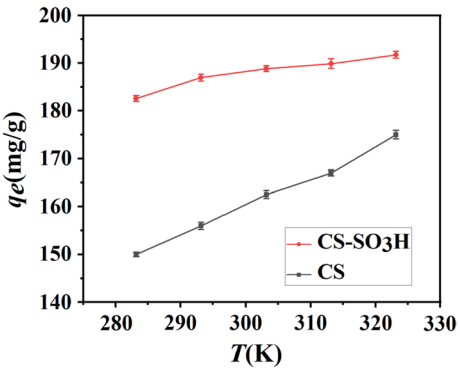

Fig. 10 Effect of temperature on the adsorption of U(VI) by CS and CS-SO_3H

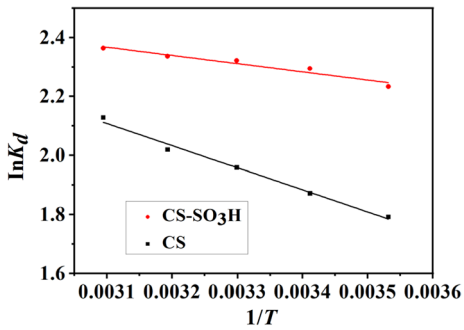

Fig. 11 Thermodynamic image of U(VI) adsorbed by CS and CS-SO_3H

adsorption capacity than CS due to the grafting of sulfonic acid groups.

Thermodynamics investigation

The adsorption capacities of uranium by CS and CS-SO_3H were investigated at five different temperatures, namely, 283.15, 293.15, 303.15, 313.15 and 323.15 K. As seen in Fig. 10, the adsorption amounts of CS and CS-SO_3H increased with temperature.

In order to explain the adsorption thermodynamic behavior, three fundamental thermodynamic parameters, namely, Gibbs free energy (ΔG; J·mol^{-1}), enthalpy change (ΔH; J·mol^{-1}) and entropy change (ΔS; J·mol^{-1}·K^{-1}), were assessed as per the following equations:

$$\ln K_d = \frac{\Delta S}{R} - \frac{\Delta H}{RT} \tag{6}$$

$$\Delta G = \Delta H = T\Delta S \tag{7}$$

where R (8.314 J·mol^{-1} K^{-1}) is the ideal gas constant and T (K) is the temperature.

The ΔH and ΔS parameters were obtained from the slope and intercept, respectively, of the plot of ln K_d versus 1/T. The results are presented in Fig. 11 and Table 4. The positive values of ΔH and the negative values of ΔG indicate the adsorption processes were endothermic and spontaneous. In addition, the absolute value of ΔG increased as temperature

Table 4 The thermodynamic parameters for U(VI) adsorbed by CS and CS-SO_3H

Materials	ΔH (kJ/mol)	ΔS (J/mol·K)	ΔG (kJ/mol)				
			283.15 K	293.15 K	303.15 K	313.15 K	323.15 K
CS	6.2293	36.8389	−4.2002	−4.5701	−4.9384	−5.3068	−5.6752
CS-SO_3H	2.3201	26.8743	−5.2893	−5.5581	−5.8268	−6.0955	−6.3643

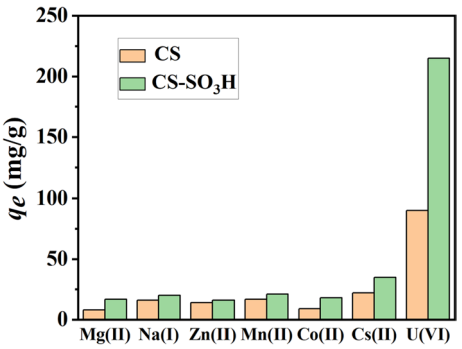

Fig. 12 Selective adsorption capacity of coexistent ions

increased, which proved that high experimental temperature was favorable to the adsorption process because of the stable adsorption sites chemically bound to U(VI). Furthermore, the positive value of Δ*S* elucidates that the randomness at the solid-solution interface augmented during the adsorption process.

Effect of coexisting ions

Considering the complex composition of nuclear wastewater, the adsorption selective properties of U(VI) by CS and CS-SO_3H in the presence of different ions, such as Mg^{2+}, Na^{+}, Zn^{2+}, Mn^{2+}, Co^{2+} and Cs^{2+}, was studied. Figure 12 shows that the influences of these ions are negligible, which proves that CS-SO_3H has good selectivity to U(VI).

Reusability study

As can be seen from Fig. 5, under lower or higher pH, the adsorption effect of U(VI) by CS-SO_3H is not ideal, thus, CS-SO_3H can be eluted with the acidic solution or alkaline solution. Figure 13a shows desorption experiments of different desorption agents. HNO_3 is the best desorption agent due to the highest desorption value. Therefore, HNO_3 was used as the adsorption agent for desorbing U(VI) in the repeated experiments, as is shown in Fig. 13b. After 5 adsorption–desorption cycles, the desorption efficiency is about 72%, which shows that CS-SO_3H has good reusability.

Possible adsorption mechanism

As exhibited in Fig. 14, compared with the XPS spectral data of CS-SO_3H, the new peak in CS-SO_3H-U spectrum is attributed to U 4f, and a small double peak appeared at 392.8 and 383.1 eV corresponding respectively to U $4f_{5/2}$ and U $4f_{7/2}$ orbitals, meaning that uranium had been combined with CS-SO_3H successfully. The spectral data of the five graphs in Fig. 13b–f were analyzed and recorded in Table 5. After uranium adsorption onto CS-SO_3H, the three peaks of quaternary-N, pyrrolidine/pyridinone-N and pyridine-N-oxide all shifted about 0.2 eV. In addition, the corresponding intensity decreased. Also, the peaks of P–O and P–C shifted about 0.1 eV and the corresponding intensity decreased. Other bonds, such as C–C and C–O, stayed the same. The results illustrate that the sulfonic acid group, P–O bonds,

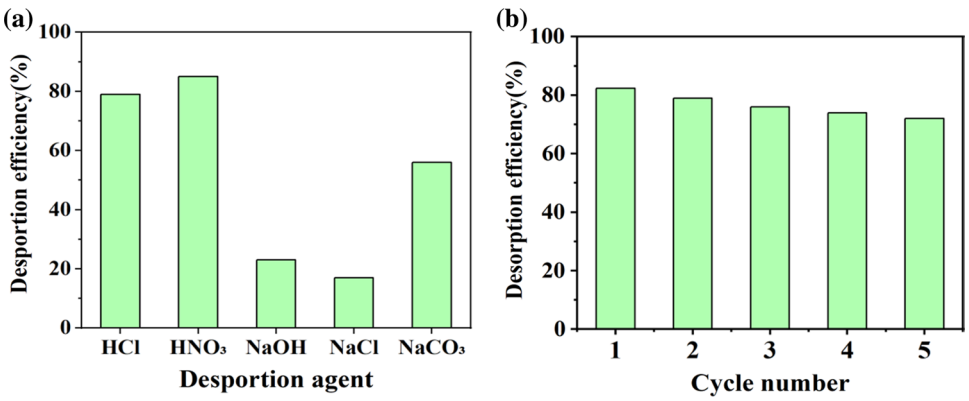

Fig. 13 (**a**) Effect of different desorption agents on U(VI) desorption. (**b**) Effect of cycle numbers on adsorption capacity of U(VI) by CS-SO_3H

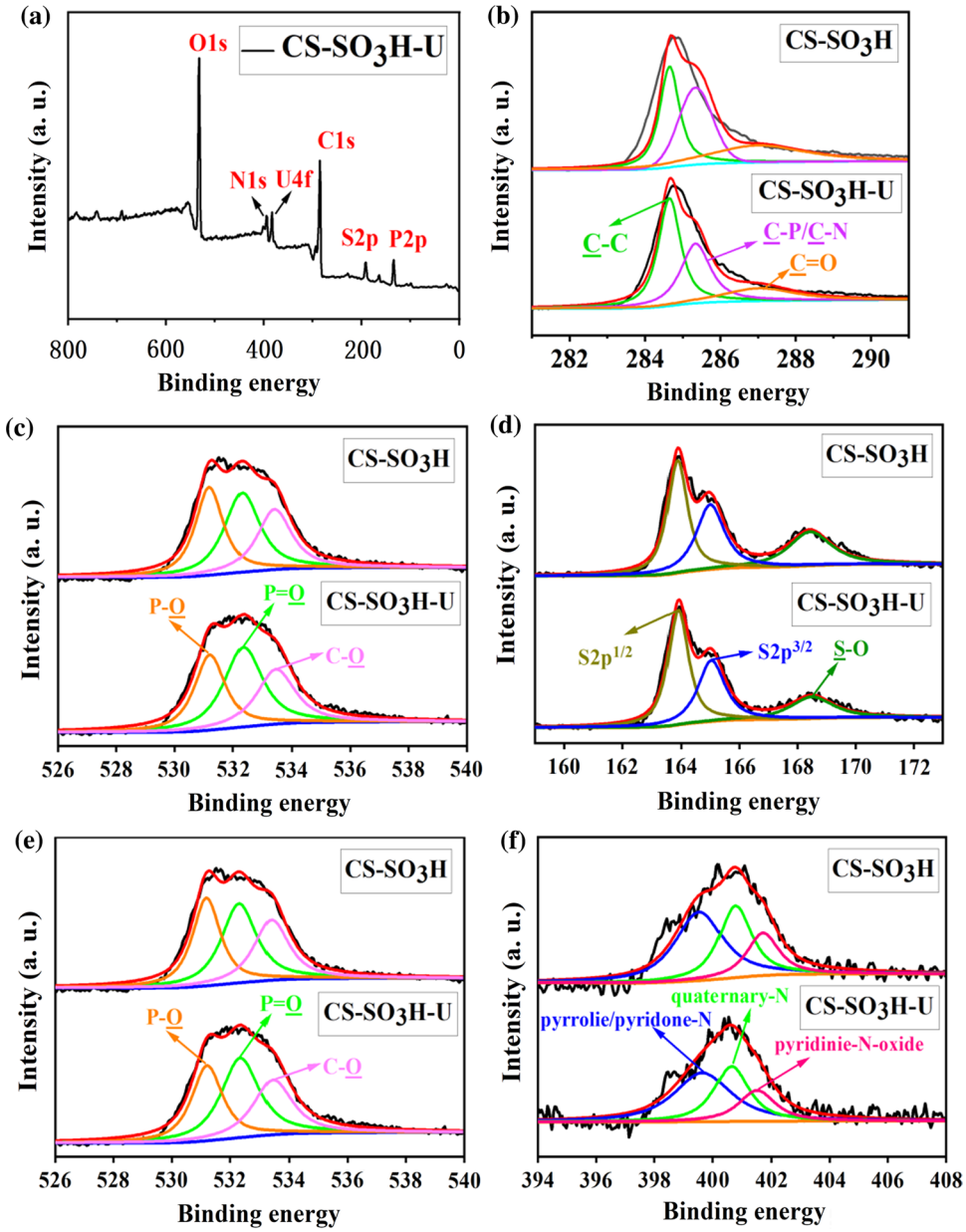

Fig. 14 XPS survey spectra of (**a**) CS-SO_3H-U; (**b**) C1s; (**c**) P2p; (**d**) S2p; (**e**) O1s and (**f**) N1s

P–C bonds and nitrogen elements in CS-SO_3H were involved in the adsorption of U(VI). According to the results of XPS and discussion of various references, the possible adsorption mechanism of U(VI) on CS-SO_3H is presented in Fig. 15.

Comparison of the adsorption capacity with other adsorbents

Table 6 shows the maximum adsorption capacity of CS-SO_3H to U(VI) compared with some reported adsorbents. It can be seen that compared with other adsorbents such as MWCA (230.3 mg/g) [23], Amidate (290 mg/g) [32], SA-GO (149.76 mg/g) [36], PCCP-AO (319.1 mg/g) [38], the adsorption capacity of CS-SO_3H for U(VI) is more prominent, indicating that CS-SO_3H can be used as a potential adsorbent for the treatment of wastewater containing U(VI).

Table 5 The data drawing list for XPS survey spectra of CS-SO_3H and CS-SO_3H-U

Materials	C element (eV)			P element (eV)		
	C–C	C–P/C–N	C = O	P–O	P–C	
CS-SO_3H	284.6	285.4	287.1	132.7	133.7	
CS-SO_3H-U	284.6	285.4	287.2	132.8	133.6	
Materials	S element (eV)			O element(eV)		
	S–O	S2p$^{1/2}$	S2p$^{3/2}$	P-O	P = O	C–O
CS-SO_3H	168.4	163.9	165	531.3	532.5	533.4
CS-SO_3H-U	168.5	164	165	531.1	532.3	533.5
Materials	N element(eV)					
	pyrrolie/pyridone-N		quaternary-N		pyridinie-N-oxide	
CS-SO_3H	399.4		400.9		401.7	
CS-SO_3H-U	399.6		400.7		401.5	

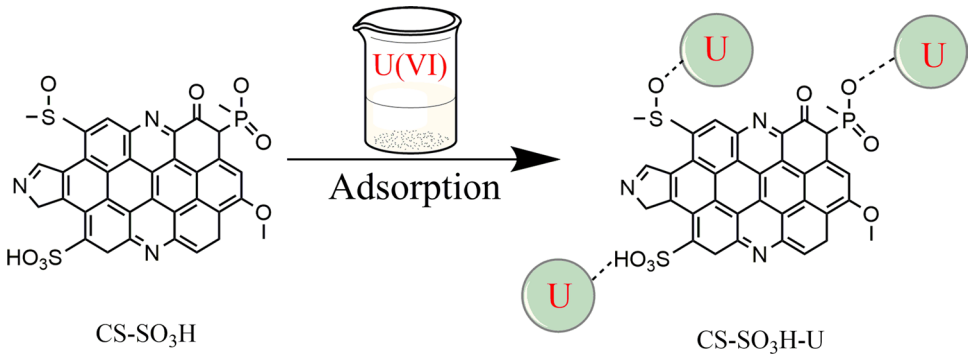

Fig. 15 Probable adsorption mechanism of U(VI) on CS-SO_3H

Table 6 Comparison of adsorption capacity by different adsorbents

Adsorbents	Solution conditions		Q_m (mg/g)	Refs.
	pH	T(K)		
MWCA	6.0	303	230.3	[23]
Amidate	6.0	298	290	[32]
SA-GO	5.0	303	149.76	[36]
MC-NH_2	5.0	298	385.98	[37]
PCCP	5.0	303	293.2	[38]
PCCP-AO	5.0	303	319.1	[38]
CS-SO_3H	6.0	298	341.98	This work

Conclusion

In summary, we synthesized sulfonic acid-functionalized carbon materials (CS-SO_3H) successfully. The adsorbent was utilized to adsorb uranium in aqueous solution and exhibited superior capacity. The experimental results indicate clearly that CS-SO_3H provided more active sites for U(VI) adsorption due to the presence of -SO_3H functional groups. Also, the co-doped P and N heteroatoms both participated in the coordination of U(VI) in the adsorption, exhibiting synergistic adsorbing effects. The results show that CS-SO_3H is an efficient adsorbent for U(VI), with significant application potential in environmental remediation.

Acknowledgements We appreciate the financial support from the National Natural Science Foundation of China (2216060121, 21966005), the Natural Science Foundation of Jiangxi Province (20202BABL203001, 20192BAB202007, 20192ACB21001), the Opening fund project of State Key Laboratory of Nuclear Resources and Environment, East China University of Technology (NRE1926), the Key Project of Science and Technology Project of Jiangxi Provincial Department of Education (GJJ200701).

References

1. Ma F, Nian J, Bi C, Yang M, Zhang C, Liu L, Dong H, Zhu M, Dong B (2019) Preparation of carboxylated graphene oxide for enhanced adsorption of U(VI). J Hazard Mater 277:9–16
2. Liao Y, Wang M, Chen DJ (2018) Production of three-dimensional porous poly-dopamine-functionalized attapulgite/chitosan aerogel for uranium(VI) adsorption. J Radioanal Nucl Ch 316:635–647
3. Chen L, Tong D (2020) Amorphous boron phosphide nanosheets: a highly efficient capacitive deionization electrode for uranium separation from seawater with superior selectivity. Sep Purif Technol 250:117175

4. Yuan Y, Yu Q, Wen J, Li C, Guo Z, Wang X, Wang N (2019) Ultrafast and highly selective uranium extraction from seawater by hydrogel-like spidroin-based protein fiber. Angew Chemie 58:11785–11790
5. Liu B, Peng T, Sun H, Yue H (2017) Release behavior of uranium in uranium mill tailings under environmental conditions. J Environ Radioactiv 171:160–168
6. Zhang X, Zhang L, Liu Y, Li M, Wu X, Jiang T, Chen C, Peng Y (2020) Mn-substituted goethite for uranium immobilization: a study of adsorption behavior and mechanism. Environ Pollut 262:114184
7. Liu X, Xu X, Sun J, Alsaedi A, Hayat T, Li J, Wang X (2018) Insight into the impact of interaction between attapulgite and graphene oxide on the adsorption of U(VI). Chem Eng J 343:217–224
8. Liu X, Sun J, Xu XT, Alsaedi A, Hayat T, Li JX (2018) Adsorption and desorption of U(VI) on different-size graphene oxide. Chem Eng J 360:941–950
9. Dong Z, Zhang Z, Zhou R, Dong Y, Wei Y, Zheng Z, Wang Y, Dai Y, Cao X, Liu Y (2020) Facile construction of Fe, N and P co-doped carbon spheres by carbothermal strategy for the adsorption and reduction of U(VI). RSC Adv 10(57):34859–34868
10. Liu Y, Zhao Z, Yuan D, Wang Y, Dai Y, Chew JW (2018) Fast and high amount of U(VI) uptake by functional magnetic CNT with phosphate group. Ind Eng Chem Res 57:14551–14560
11. Wu W, Chen D, Li J, Su M, Chen N (2018) Enhanced adsorption of uranium by modified red mud: adsorption behavior study. Environ Sci Pollut R 25(18):18096–18108
12. Liu Y, Dai Y, Yuan D, Wang Y, Zou L (2017) The preparation of PZS-OH/CNT composite and its adsorption of U(VI) in aqueous solutions. J Radioanal Nucl Ch 314(3):1747–1757
13. Abdi S, Nasiri M, Mesbahi A, Khani MH (2017) Investigation of uranium (VI) adsorption by polypyrrole. J Hazard Mater 332:132–139
14. Burns AD, Abbasi P, Dreisinger DB (2016) Uranous sulfate precipitation as a novel hydrometallurgical process for uranium purification. Hydrometallurgy 163:49–54
15. Shi S, Qian YX, Mei PP, Yuan YH, Jia N, Dong MY, Fan JC, Guo ZH, Wang N (2020) Robust flexible poly(amidoxime) porous network membranes for highly efficient uranium extraction from seawater. Nano Energy 71:104629
16. Chen Y, Wei Y, He L, Tang F (2016) Separation of thorium and uranium in nitric acid solution using silica based anion exchange resin. J Chromatogr A 1466:37–41
17. Shen J, Schäfer A (2014) Removal of fluoride and uranium by nanofiltration and reverse osmosis: a review. Chemosphere 117:679–691
18. Wang G, Liu J, Wang X, Xie Z, Deng N (2009) Adsorption of uranium (VI) from aqueous solution onto cross-linked chitosan. J Hazard Mater 168(2–3):1053–1058
19. Xie CY, Jing SP, Wang Y, Lin X, Bao HL, Guan CZ, Jin C, Wang JQ (2017) Adsorption of uranium (VI) onto amidoxime-functionalized ultra-high molecular weight polyethylene fibers from aqueous solution. Nucl Sci Tech 28(7):97–104
20. Chen Z, Song C, Sun X, Guo H, Zhu G (2011) Kinetic and isotherm studies on the electro-sorption of NaCl from aqueous solutions by activated carbon electrodes. Desalination 267(2–3):239–243
21. Jo H, Kim KH, Jung MJ, Park JH, Lee YS (2017) Fluorination effect of activated carbons on performance of asymmetric capacitive deionization. Appl Surf Sci 409:117–123
22. Zhang Y, Ye T, Wang Y, Zhou L, Liu Z (2021) Adsorption of uranium (VI) from aqueous solution by phosphorylated luffa rattan activated carbon. J Radioanal Nucl Ch 327:1267–1275
23. Yin N, Ai Y, Xu Y, Ouyang Y, Yang P (2020) Preparation of magnetic biomass-carbon aerogel and its application for adsorption of uranium(VI). J Radioanal Nucl Ch 326:1307–1321
24. Zhang H, Zhang J (2020) The preparation of novel polyvinyl alcohol (PVA)-based nanoparticle/carbon nanotubes (PNP/CNTs) aerogel for solvents adsorption application. J Coll Interf Sci 569:254–266
25. Zhang Z, Qiu Y, Dai Y, Wang P, Gao B, Dong Z, Cao X, Liu Y, Le Z (2016) Synthesis and application of sulfonated graphene oxide for the adsorption of uranium(VI) from aqueous solutions. J Radioanal Nucl Ch 310(2):547–557
26. Balarak D, Mostafapour F, Bazrafshan E, Saleh TA (2017) Studies on the adsorption of amoxicillin on multi-wall carbon nanotubes. Water Sci Technol 75(7):1599–1606
27. Wei XJ, Li XJ, Lv CC, Mo XP, Li KX (2020) Hierarchically yolk-shell porous carbon sphere as an electrode material for high-performance capacitive deionization. Electrochim Acta 354:136590
28. Liu XP, Liu Y, Wang Y, Yuan D, Liu J, Chew JW (2021) Preparation of porous carbon materials by polyphosphazene as precursor for sorption of U(VI). Coll Interf Sci 41:100387
29. Pagano JK, Arney DSJ, Scott B, Morris D, Kiplinger J, Burns C (2018) A sulphur and uranium fiesta! Synthesis, structure, and characterization of neutral terminal uranium(VI) monosulphide, uranium(VI) η2-disulphide, and uranium(IV) phosphine sulphide complexes. Dalton Trans 48(1):50–57
30. Jiang C, Liu Y, Yuan D, Wang Y, Liu J, Chew JW (2020) Investigation of the high U(VI) adsorption properties of phosphoric acid-functionalized heteroatoms-doped carbon materials. Solid State Sci 104:106248
31. Li Z, Chen C, McCaffrey M, Yang H, Allcock HR (2020) Polyphosphazene elastomers with alkoxy and trifluoroethoxy side groups. ACS Appl Polym Mater 2:475–480
32. Liu Y, Ouyang Y, Huang D, Jiang C, Liu X, Wang Y, Dai Y, Yuan D, Chew JW (2020) N, P and S co-doped carbon materials derived from polyphosphazene for enhanced selective U(VI) adsorption. Sci Total Environ 706:136019
33. Liu Y, Zhao Z, Yuan D, Wang Y, Dai Y, Zhu Y, Chew JW (2019) Introduction of amino groups into polyphosphazene framework supported on CNT and coated Fe3O4 nanoparticles for enhanced selective U(VI) adsorption. Appl Surf Sci 466:893–902
34. Du CY, Zhao TS, Liang ZX (2007) Sulfonation of carbon-nanotube supported platinum catalysts for polymer electrolyte fuel cells. J Power Sour 176(1):9–15
35. Xing R, Liu N, Liu Y, Wu H, Jiang Y, Chen L, He M, Wu P (2007) Novel solid acid catalysts: sulfonic acid group-functionalized mesostructured polymers. Adv Funct Mater 17(14):2455–2461
36. Li D, Zhang P, Yang Y, Huang Y, Li T, Yang J (2021) U(VI) adsorption by sodium alginate/graphene oxide composite beads in water. J Radioanal Nucl Ch 327:1131–1141
37. Wang Y, Yu C, Zeng D, Zhang Z, Cao X, Liu Y (2021) High-efficiency removal of U(VI) by mesoporous carbon functionalized with amino group. J Radioanal Nucl Ch 328:951–961
38. Cui M, Xiang S, Zhang S, Long T, Luo Z, Yang H (2021) Amidoximated polyorganophosphazene microspheres with an excellent property of U(VI) adsorption in aqueous solution. J Radioanal Nucl Ch 328:1161–1172